2600 *Inorg. Chem.* **2010**, *49*, 2600–2613
DOI: 10.1021/ic901113p

Inorganic Chemistry
Article

Hierarchical Assembly of Extended Coordination Networks Constructed by Novel Metallacalix[4]arenes Building Blocks

Xia Li, Benlai Wu,* Ruiying Wang, Hongyun Zhang,* Caoyuan Niu, Yunyin Niu, and Hongwei Hou

Department of Chemistry, Zhengzhou University, Zhengzhou 450052, People's Republic of China

Received June 9, 2009

Five interesting metal−organic nanostructures and networks, $[Ni_4(HL)_4(bpy)(py)(H_2O)_5]_2\cdot 0.5H_2O$ (**1**), $[Co_4(HL)_4(bpy)(py)(H_2O)_5]_2\cdot 0.5H_2O$ (**2**), $[Ni_4(HL)_4(H_2O)_7]_n\cdot nH_2O$ (**3**), $[Ni_4(HL)_4(bpy)_2(H_2O)_4]_n$ (**4**), and $[Cd_4(HL)_4(H_2O)]_n$ (**5**), were synthesized hydrothermally [H_3L = 2-(pyridin-2-yl)-1*H*-imidazole-4,5-dicarboxylate acid, py = pyridine, and bpy = 4,4′-bipyridine]. Intriguingly, all compounds consist of novel metallacalix[4]arene building blocks $M_4(HL)_4$, where doubly deprotonated HL in the same bichelating fashion of μ-*k*N,N′:*k*O,N″ displays a strong coordination orientation by cooperation of the 4,5-imidazoledicarboxylate and 2-pyridyl groups. Very interestingly, the symmetry of $M_4(HL)_4$ and the linkage styles between metal nodes and HL in $M_4(HL)_4$ are sensitive to the reaction conditions, and the resulting structural motifs vary with secondary ligands and metal nodes. In **1** and **2**, two C_1-symmetric $M_4(HL)_4$ units are bpy-bridged into dimeric chiral nanomolecules with two different cavities. As deprotonated with NaOH, the combination of Ni^{II} and HL forms a pseudo-S_4- or S_4-symmetric $M_4(HL)_4$, which further assembles into 1D chiral crystals **3** or rare 3D crystals **4** of bpy-bridged 5-fold interpenetrating diamondoid architecture with metallacalix[4]arene building blocks as novel 4-connecting nodes, and the combination of Cd^{II} and HL forms an 8-connected C_2-symmetric $M_4(HL)_4$ that fabricates the α-Po net of **5**. Notably, those large $M_4(HL)_4$ units are potentially highly connected building blocks in a hierarchical assembly of metal−organic networks. Magnetic studies disclose antiferromagnetic interactions in $M_4(HL)_4$ of **1**−**4**. The magnetic data for **1**, **3**, and **4**, all containing isomeric $Ni_4(HL)_4$ units, are analyzed by an equilateral quadrangle isotropic model combined with the molecular-field approximation with $J = -4.00(2)$, $-3.39(2)$, and $-2.72(3)$ cm^{-1}, respectively, presenting a stronger comparison between the structure and magnetism. The emission of **5** is odd, which perhaps is relative to the bichelating fashion of ligand HL and a rare coordination geometry of Cd^{II}. Moreover, the thermal stability and gas sorption properties of these compounds were measured.

Introduction

Metal−organic materials built from the node−linker combination strategy are extremely promising in many areas, such as catalysis, sensing, magnetism, and ion exchange.[1] So far, metal−organic frameworks (MOFs) with more flexible rational designs through control of the dimensions, structural topologies, and functional pores have particularly drawn recent attention because of their great potential applications as microporous, magnetic, nonlinear optical, and fluorescent materials.[2−4] Except for the usual utilization of metal ions as nodes, an innovative route toward the construction of functional MOFs is the use of molecular building blocks (MBBs) as nodes/spacers, which are most commonly metal-containing aggregates that dictate the direction of polymer extension through their steric requirements and rigidity.[5]

*To whom correspondence should be addressed. E-mail: wbl@zzu.edu.cn (B.W.), wzhy917@zzu.edu.cn (H.Z.). Tel.: +86 0371 67763675.

(1) (a) Kitagawa, S.; Kitaura, R.; Noro, S. I. *Angew. Chem., Int. Ed.* **2004**, *43*, 2334. (b) Janiak, C. *Dalton Trans.* **2003**, 2781. (c) Seo, J. S.; Whang, D.; Lee, H.; Jun, S. I.; Oh, J.; Jeon, Y. J.; Kim, K. *Nature* **2000**, *404*, 982. (d) Evans, O. R.; Xiong, R.-G.; Wang, Z.-Y.; Wong, G.-K.; Lin, W.-B. *Angew. Chem., Int. Ed.* **1999**, *38*, 536. (e) Sun, J.; Weng, L.; Zhou, Y.; Chen, J.; Chen, Z.; Liu, Z.; Zhao, D. *Angew. Chem., Int. Ed.* **2002**, *41*, 4471. (f) Yaghi, O. M.; O'Keeffe, M.; Ockwig, N. W.; Chae, H. K.; Eddaoudi, M.; Kim, J. *Nature* **2003**, *423*, 705.

(2) (a) Wang, L.-Y.; Yang, Y.; Liu, K.; Li, B.-L.; Zhang, Y. *Cryst. Growth Des.* **2008**, *8*, 3902. (b) Rowsell, J. L. C.; Millward, A. R.; Park, K. S.; Yaghi, O. M. *J. Am. Chem. Soc.* **2004**, *126*, 5666. (c) Wu, C.-D.; Hu, A.-G.; Zhang, L.; Lin, W.-B. *J. Am. Chem. Soc.* **2005**, *127*, 8940. (d) Fujita, M.; Kwon, Y. J.; Washizu, S.; Ogura, K. *J. Am. Chem. Soc.* **1994**, *116*, 1151. (e) Moulton, B.; Zaworotko, M. J. *Chem. Rev.* **2001**, *101*, 1629. (f) McKinlay, A. C.; Xiao, B.; Wragg, D. S.; Wheatley, P. S.; Megson, I. L.; Morris, R. E. *J. Am. Chem. Soc.* **2008**, *130*, 10440.

(3) Navarro, J. A. R.; Barea, E.; Salas, J. M.; Masciocchi, N.; Galli, S.; Sironi, A.; Ania, C. O.; Parra, J. B. *Inorg. Chem.* **2006**, *45*, 2397.

(4) (a) Eddaoudi, M.; Moler, D. B.; Li, H.; Chen, B.; Reineke, T. M.; O'Keeffe, M.; Yaghi, O. M. *Acc. Chem. Res.* **2001**, *34*, 319. (b) Kuznicki, S. M.; Bell, V. A.; Nair, S.; Hillhouse, H. W.; Jacubinas, R. M.; Braunbarth, C. M.; Toby, B. H.; Tsapatsis, M. *Nature* **2001**, *412*, 720. (c) Christian, S.; Fabienne, P.; Nicole, G.; Férey, G. *Chem. Mater.* **2004**, *16*, 1177. (d) Johnson, J. A.; Kamf, J. W.; Pecoraro, V. L. *Angew. Chem., Int. Ed.* **2003**, *42*, 546.

(5) (a) Moulton, B.; Zaworotko, M. J. *Chem. Rev.* **2001**, *101*, 1629. (b) Seidel, S. R.; Stang, P. J. *Acc. Chem. Res.* **2002**, *35*, 972. (c) Cotton, F. A.; Lin, C.; Murillo, C. A. *Acc. Chem. Res.* **2001**, *34*, 759. (d) McManus, G. J.; Wang, Z. Q.; Beauchamp, D. A.; Zaworotko, M. J. *Chem. Commun.* **2007**, 5212. (e) Liu, Y. L.; Kravtsov, V. C.; Beauchamp, D. A.; Eubank, J. F.; Eddaoudi, M. *J. Am. Chem. Soc.* **2005**, *127*, 7266. (f) Dybtsev, D. N.; Chun, H.; Yoon, S. H.; Kim, D.; Kim, K. *J. Am. Chem. Soc.* **2004**, *126*, 32. (g) Kubota, Y.; Takata, M.; Matsuda, R.; Kitaura, R.; Kitagawa, S.; Kato, K.; Sakata, M.; Kobayashi, T. C. *Angew. Chem., Int. Ed.* **2005**, *44*, 920.

Published on Web 02/08/2010

Multifunctional connector 4,5-imidazoledicarboxylic acid (H_3IDC), by adjustment of its existing forms and coordination models through pH or temperature in assembly reaction systems, shows more interesting traits in the construction of nanostructures and MOFs and thus has been extensively investigated in coordination chemistry.[6] Intriguingly, its two nitrogen atoms in the imidazole ring can gear the coordination orientation, sometimes strengthened by the cooperative coordination of the adjacent carboxylic groups, to produce large stable MBBs, such as cagelike,[6a] cubic,[6b,c] or tetrahedral metal-containing aggregates,[6d] which can be reticulated into novel metal−organic topologies with special catalysis or porosity. In this context, our group has onset a program to engraft various pyridyl groups into the backbone of H_3IDC at the 2 position. The further functionalized derivatives completely retaining the gracious coordination block 4,5-imidazoledicarboxylic group were expected not only to inherit the outstanding coordination properties in fabricating novel MBBs that direct the resultant assemblies into novel MOF materials like those in H_3IDC complexes but also to subtly tune and/or enhance the respective properties of ligands and MOFs through the collaboration of the pyridyl and 4,5-imidazoledicarboxylic groups. Very recently, we have reported several 2D and 3D MOFs of 2-(pyridin-4-yl)-1*H*-imidazole-4,5-dicarboxylic acid (H_3PIDC) in which the doubly deprotonated ligand HPIDC adopted μ_3- or μ_4-coordination modes.[7] Structural analyses projected the coordination orientation of the 4,5-imidazoledicarboxylate group and obvious structure diversity tuned by the coordination of 4-pyridyl. However, it seemed very slight to generate MBBs through the cooperative orientation of the 4,5-imidazoledicarboxylate and 4-pyridyl groups. Perhaps, it is due to the fairly separated distances of bites embedded in the 4,5-imidazoledicarboxylate and 4-pyridyl groups, which restrain them to work together well like that of the rigid planar ligand H_3IDC. In our continuing effort in this field, another analogue of 4,5-imidazoledicarboxylic acid, namely, 2-(pyridin-2-yl)-1*H*-imidazole-4,5-dicarboxylate acid (H_3L), has been employed, given that its 4,5-imidazoledicarboxylate and 2-pyridyl groups can jointly exert influence upon the coordination orientation through chelation with the same metal node. Here we report the syntheses, structures, and porous properties of five coordination complexes, $[Ni_4(HL)_4(bpy)(py)(H_2O)_5]_2\cdot 0.5H_2O$ (**1**), $[Co_4(HL)_4(bpy)(py)(H_2O)_5]_2\cdot 0.5H_2O$ (**2**), $[Ni_4(HL)_4(H_2O)_7]_n\cdot nH_2O$ (**3**), $[Ni_4(HL)_4(bpy)_2(H_2O)_4]_n$ (**4**), and $[Cd_4(HL)_4(H_2O)]_n$ (**5**), where bpy = 4,4′-bipyridine and py = pyridine. In those nanostructures/MOFs, a doubly deprotonated 2-(pyridin-2-yl)-imidazol-4,5-dicarboxylate system as an exotetradentate ligand is able to build interesting cyclic tetranuclear building blocks $M_4(HL)_4$ ($M = Ni^{2+}$, Co^{2+}, or Cd^{2+}), which were termed as metallacalix[4]arenes by Navorro et al. because they are very similar in conformation to purely organic calix[4]arenes,[3,8] and those novel metallacalix[4]arene building blocks can be further assembled with additional connecting ligands to build extended structures.

Experimental Section

General Remarks. All chemicals purchased were of reagent grade or better and were used without further purification. The H_3L ligand was prepared by the method reported in the literature.[9] Element analyses were performed with a Carlo-Erba 1106 elemental analyzer. IR spectra were recorded on a Bruker VECTOR22 spectrophotometer with KBr pellets in the 400−4000 cm^{-1} region. Thermal analysis curves were scanned in the range of 30−600 °C with an air atmosphere on a STA 409 PC thermal analyzer. Nitrogen adsorption isotherms were taken on a Shimadzu ASAP2010. Powder X-ray diffraction (PXRD) patterns of the samples were recorded by a Rigaku DMAX2500 X-ray diffractometer with Cu Kα radiation. The temperature-dependent magnetic measurements were determined on a Quantum Design SQUID-XL7 magnetometer.

Synthesis. Syntheses of the compounds were achieved by a hydrothermal technique in a Teflon-lined autoclave under synthetic reaction conditions determined empirically.

$[Ni_4(HL)_4(bpy)(py)(H_2O)_5]_2\cdot 0.5H_2O$ (1). A mixture of $Ni(NO_3)_2\cdot 6H_2O$ (0.0291 g, 0.1 mmol), H_3L (0.0233 g, 0.1 mmol), bpy (0.0198 g, 0.1 mmol), py (0.2 mL), and H_2O (10 mL) sealed into a Teflon-lined stainless autoclave had been heated at 160 °C for 3 days. After a gradual cooling to room temperature, green block crystals were obtained in 60% yield (based on Ni). Elem anal. Calcd for $C_{110}H_{87}N_{30}Ni_8O_{42.5}$: C, 44.43; H, 2.95; N, 14.14. Found: C, 44.61; H, 2.93; N, 14.24. IR data (KBr pellet, ν [cm^{-1}]): 3098 (b), 1676 (m), 1615 (s), 1530 (s), 1499 (s), 1478 (s), 1419 (m), 1370 (m), 1268 (m), 1226 (m), 1155 (m), 1123 (m), 1068 (m), 867 (m), 794 (m), 720 (m), 635 (m), 573 (m), 532 (m).

$[Co_4(HL)_4(bpy)(py)(H_2O)_5]_2\cdot 0.5H_2O$ (2). Following the same synthetic procedure of **1**, red block crystals of **2** were obtained through the replacement of $Ni(NO_3)_2\cdot 6H_2O$ with $Co(NO_3)_2\cdot 6H_2O$. Yield: 67% (based on Co). Elem anal. Calcd for $C_{110}H_{87}N_{30}Co_8O_{42.5}$: C, 44.31; H, 2.94; N, 14.10. Found: C, 44.74; H, 2.91; N, 14.30. IR data (KBr pellet, ν [cm^{-1}]): 3405 (b), 1608 (m), 1533 (s), 1498 (s), 1420 (m), 1373 (m), 1268 (m), 1157 (m), 1122 (m), 1022 (m), 866 (m), 799 (m), 721 (m), 631 (m), 569 (m), 529 (m).

$[Ni_4(HL)_4(H_2O)_7]_n\cdot nH_2O$ (3). A mixture of $Ni(NO_3)_2\cdot 6H_2O$ (0.0291 g, 0.1 mmol), H_3L (0.0233 g, 0.1 mmol), NaOH (0.0080 g, 0.2 mmol), and H_2O (10 mL) sealed into a Teflon-lined stainless autoclave had been heated at 160 °C for 3 days. After a gradual cooling to room temperature, green block crystals were obtained in 40% yield (based on Ni). Elem anal. Calcd for $C_{40}H_{36}N_{12}Ni_4O_{24}$: C, 36.92; H, 2.79; N, 12.93. Found: C, 37.14; H, 2.72; N, 12.98. IR data (KBr pellet, ν [cm^{-1}]): 3406 (b), 1646 (m), 1612 (m), 1546 (s), 1501 (s), 1378 (s), 1272 (m), 1157 (m), 1122 (m), 1025 (m), 871 (m), 798 (m), 716 (m), 573 (m), 536 (m).

$[Ni_4(HL)_4(bpy)_2(H_2O)_4]_n$ (4). A mixture of $Ni(NO_3)_2\cdot 6H_2O$ (0.0291 g, 0.1 mmol), H_3L (0.0233 g, 0.1 mmol), bpy (0.0198 g, 0.1 mmol), NaOH (0.0080 g, 0.2 mmol), and H_2O (10 mL) sealed

(6) (a) Lu, W.-G.; Su, C.-Y.; Lu, T.-B.; Jiang, L.; Chen, J.-M. *J. Am. Chem. Soc*. **2006**, *128*, 34. (b) Zou, R.-Q.; Sakurai, H.; Xu, Q. *Angew Chem., Int. Ed*. **2006**, *45*, 2542. (c) Zou, R.-Q.; Jiang, L.; Senoh, H.; Takeichi, N.; Xu, Q. *Chem. Commun*. **2005**, 3526. (d) Liu, Y.-L.; Kravtsov, V. C.; Larsen, R.; Eddaoudi, M. *Chem. Commun*. **2006**, 1488. (e) Sun, Y.-Q.; Zhang, J.; Chen, Y.-M.; Yang, G.-Y. *Angew. Chem., Int. Ed*. **2005**, *44*, 5814. (f) Maji, T. K.; Mostafa, G.; Chang, H. C.; Kitagawa, S. *Chem. Commun*. **2005**, 2436. (g) Liu, Y.-L.; Kravtsov, V.; Walsh, R. D.; Poddar, P.; Srikanth, H.; Eddaoudi, M. *Chem. Commun*. **2004**, 2806. (h) Rajendiran, T. M.; Kirk, M. L.; Setyawati, I. A.; Caudle, M. T.; Kampf, J. W.; Pecoraro, V. L. *Chem. Commun*. **2003**, 824. (i) Plieger, P. G.; Ehler, D. S.; Duran, B. L.; Taylor, T. P.; John, K. D.; Keizer, T. S.; McCleskey, T. M.; Burrell, A. K.; Kampf, J. W.; Haase, T.; Rasmussen, P. G.; Karr, J. *Inorg. Chem*. **2005**, *44*, 5761. (j) Li, C.-J.; Hu, S.; Li, W.; Lam, C. K.; Zheng, Y.-Z.; Tong, M.-L. *Eur. J. Inorg. Chem*. **2006**, 1931. (k) Gu, J.-Z.; Lu, W.-G.; Jiang, L.; Zhou, H.-C.; Lu, T.-B. *Inorg. Chem*. **2007**, *46*, 5835. (l) Fang, R.-Q.; Zhang, X.-M. *Inorg. Chem*. **2006**, *45*, 4801. (m) Wang, Y.-L.; Yuan, D.-Q.; Bi, W.-H.; Li, X.; Li, X. J.; Li, F.; Cao, R. *Cryst. Growth Des*. **2005**, *5*, 1849.

(7) Li, X.; Wu, B.-L.; Niu, C.-Y.; Niu, Y.-Y.; Zhang, H.-Y. *Cryst. Growth Des*. **2009**, *9*, 3423.

(8) Navarro, J. A. R.; Bareaa, E.; Galindoa, M. A.; Salasa, J. M.; Romeroa, M. A.; Quirósa, M.; Masciocchib, N.; Gallib, S.; Sironic, A.; Lippertd, B. *J. Solid State Chem*. **2005**, *178*, 2436.

(9) Spek, A. L. J. *Appl. Crystallogr*. **2003**, *36*, 7.

Table 1. Crystal Data and Structure Refinement for Complexes **1**−**5**

	1	**2**	**3**	**4**	**5**
formula	$C_{110}H_{87}N_{30}Ni_8O_{42.5}$	$C_{110}H_{87}Co_8N_{30}O_{42.5}$	$C_{40}H_{36}N_{12}Ni_4O_{24}$	$C_{60}H_{44}N_{16}Ni_4O_{20}$	$C_{40}H_{24}Cd_4N_{12}O_{18}$
fw	2978.78	2980.54	1303.65	1543.95	1410.31
cryst syst	monoclinic	monoclinic	orthorhombic	tetragonal	orthorhombic
space group	$C2/c$	$C2/c$	$P2_12_12_1$	$I4_1/a$	$Pbcn$
a (Å)	32.347(3)	32.8249(19)	11.495(2)	14.0670(7)	11.1662(10)
b (Å)	11.0256(11)	11.1266(7)	14.426(3)	14.0670(7)	26.553(2)
c (Å)	40.637(4)	40.606(2)	28.924(6)	39.336(4)	14.4125(13)
α (deg)	90	90	90	90	90
β (deg)	110.3480(10)	110.6420(10)	90	90	90
γ (deg)	90	90	90	90	90
V (Å^3)	13588(2)	13878.3(14)	4796.2(17)	7783.8(9)	4273.2(7)
Z	4	4	4	4	4
D_{calcd} (g cm^{-3})	1.456	1.426	1.805	1.317	2.192
$F(000)$	6084	6052	2656	3152	2736
θ range (deg)	2.35−25.00	2.33−25.00	1.58−24.99	2.91−24.99	2.43−28.33
index range (deg)	$-38 \le h \le 38$, $-13 \le k \le 13$, $-48 \le l \le 48$	$-38 \le h \le 38$, $-13 \le k \le 13$, $-48 \le l \le 48$	$-13 \le h \le 13$, $-17 \le k \le 17$, $-35 \le l \le 35$	$-16 \le h \le 16$, $-16 \le k \le 16$, $-46 \le l \le 46$	$-14 \le h \le 14$, $-35 \le k \le 34$, $-19 \le l \le 19$
reflns collected/ unique (R_{int})	47 166/11 661 (R_{int} = 0.0450)	47 492/11 772 (R_{int} = 0.0466)	48 684/8433 (R_{int} = 0.0475)]	27 772/3349 (R_{int} = 0.0610)	37 600/5320 (R_{int} = 0.0492)
GOF on F^2	1.038	1.036	1.081	1.078	1.024
R1, wR2 [$I > 2\sigma(I)$]	0.0537, 0.1450	0.0601, 0.1611	0.0330, 0.0683	0.0660, 0.1872	0.0290, 0.0579
R1, wR2 (all data)	0.0750, 0.1631	0.0835, 0.1820	0.0346, 0.0713	0.0825, 0.2067	0.0490, 0.0653
largest difference in peak and hole (e Å^{-3})	1.131, −0.426	1.292, −0.650	0.358, −0.327	1.445, −0.477	0.793, −0.621

into a Teflon-lined stainless autoclave had been heated at 160 °C for 3 days. After a gradual cooling to room temperature, green rhombus crystals were obtained in 40% yield (based on Ni). Elem anal. Calcd for $C_{60}H_{44}N_{16}Ni_4O_{20}$: C, 46.75; H, 2.88; N, 14.55. Found: C, 46.98; H, 2.80; N, 14.68. IR data (KBr pellet, ν [cm^{-1}]): 3398 (b), 1686 (m), 1610 (m), 1530 (s), 1499 (s), 1478 (s), 1421 (m), 1373 (m), 1268 (m), 1220 (m), 1157 (m), 1123 (m), 1068 (m), 867 (m), 798 (m), 718 (m), 633 (m), 571 (m), 530 (m).

$[Cd_4(HL)_4(H_2O)]_n$ (5). Following the same synthetic procedure of **1**, colorless block crystals of **5** were obtained through the replacement of $Ni(NO_3)_2\cdot 6H_2O$ with $Cd(NO_3)_2\cdot 6H_2O$. Yield: 53% (based on Cd). Elem anal. Calcd for $C_{40}H_{24}Cd_4N_{12}O_{18}$: C, 33.90; H, 1.71; N, 11.87. Found: C, 34.12; H, 1.68; N, 11.98. IR data (KBr pellet, ν [cm^{-1}]): 3524 (b), 3085 (b), 1698 (s), 1559 (s), 1494 (m), 1362 s), 1270 (s), 1126 (m), 1017 (m), 852 (m), 798 (m), 753 (m), 715 (m), 638 (m), 567 (m), 528 (m).

X-ray Structure Determination. Crystallographic data for compounds **1**−**5** were collected at 291(2) K on a Bruker SMART APEX-II CCD diffractometer equipped with a graphite crystal and incident beam monochromator using Mo Kα radiation (λ = 0.710 73 Å). Absorption corrections were applied by using *SADABS*. The structures were solved with direct methods and refined with full-matrix least-squares techniques on F^2 using the *SHELXTL* program package.[10] The nonhydrogen atoms were refined anisotropically. The hydrogen atoms were treated as idealized contributions except water molecules, whose hydrogen atoms were located from difference Fourier maps and included in the final refinement by using geometrical restraints. Crystal data are summarized in detail in Table 1. Selected bond lengths and bond angles are listed in Table 2. Hydrogen bond data of complex **3** are listed in Table 3. Crystallographic data for the structural analysis have been deposited with the Cambridge Crystallographic Data Centre, CCDC 725525−725529 for **1**−**5**. Copies of this information may be obtained free of charge at www.ccdc.cam.ac.uk/conts/retrieving.html or from the Cambridge Crystallographic Data Centre, 12 Union Road, Cambridge CB21EZ, U.K. [fax (+44) 1223-336-033; e-mail deposit@ccdc.cam.ac.uk].

(10) Sheldrick, G. M. *Bruker SHELXTL-PC*; University of Göttingen: Göttingen, Germany, 1997.

Results and Discussion

Synthesis and Coordination Modes. All compounds were prepared hydrothermally at 160 °C. Ligand H_3L was doubly deprotonated in the construction of all complexes and presents four coordination modes (Scheme 1). In all compounds, ligands HL in a bichelating fashion bridge metal nodes to form the basic metallacalix[4]arene building blocks $M_4(HL)_4$ (M = Ni^{2+}, Co^{2+}, or Cd^{2+}). In the calix[4]arene analogues, the phenol and methylene groups have been displaced by HL and metal nodes, respectively. The structural motifs of the resulting complexes vary with the secondary ligands and metal nodes. Very interestingly, the symmetry of $M_4(HL)_4$ and the linkage styles between the metal nodes and HL ligands in $M_4(HL)_4$ are sensitive to reaction conditions (Scheme 2). As deprotonated with py, Co^{II} or Ni^{II} centers are linked by HL in the A mode to form a C_1-symmetric $M_4(HL)_4$, which is bpy-bridged into dimeric **1** or **2**. However, as deprotonated with NaOH, the combination of Ni^{II} and HL in the B mode forms a pseudo-S_4- or S_4-symmetric $M_4(HL)_4$, which further assembles into the 1D helix polymer **3** or the bpy-bridged 3D diamondoid architecture **4**, and the combination of Cd^{II} and HL in the C mode forms a C_2-symmetric $M_4(HL)_4$ in the α-Po net of **5**. Although no further deprotonation took place when NaOH was used instead of py, py in the reaction systems acts as not only a base to deprotonate but also a rival terminal ligand. In our opinions, besides the flexible coordination modes of the metal centers and the distortion of the coordination geometry, the partial habitation of the coordination sites around the individual metal centers by py in the resulting metallacalix[4]arene $M_4(HL)_4$ units can effect the linkage styles between the metal nodes and HL ligands through steric hindrance and degrade the symmetry of the coordination geometry fabricated by more multifold ligands as well as the symmetry of the resulting metallacalix[4]arene $M_4(HL)_4$ units.

Table 2. Selected Bond Distances (Å) and Angles (deg) for Complexes **1**−**5**[a]

				1			
Ni1−O16	2.038(3)	Ni1−O1	2.022(3)	Ni1−O17	2.087(3)	Ni1−N13	2.129(4)
Ni1−N1	2.166(3)	Ni1−N12	2.179(3)	Ni2−O18	2.051(3)	Ni2−O5	2.089(3)
Ni2−N3	2.088(4)	Ni2−N15	2.118(4)	Ni2−N2	2.124(3)	Ni2−N4	2.126(3)
Ni3−O19	2.037(4)	Ni3−O20	2.047(4)	Ni3−N7	2.095(4)	Ni3−N6	2.105(4)
Ni3−N8	2.125(3)	Ni3−N5	2.128(3)	Ni4−O21	2.054(4)	Ni4−O12	2.070(3)
Ni4−N10	2.075(4)	Ni4−N14#1	2.114(4)	Ni4−N11	2.114(4)	Ni4−N9	2.170(3)
O16−Ni1−N12	79.86(12)	O1−Ni1−N1	79.59(12)	N3−Ni2−N2	79.90(13)	O5−Ni2−N4	78.73(12)
N7−Ni3−N8	79.50(13)	N6−Ni3−N5	79.59(14)	O12−Ni4−N9	78.71(12)	N10−Ni4−N11	79.43(14)
				2			
Co1−O1	2.057(3)	Co1−O16	2.068(3)	Co1−O17	2.114(3)	Co1−N1	2.194(3)
Co1−N13	2.196(4)	Co1−N12	2.217(4)	Co2−O18	2.075(3)	Co2−N15	2.131(4)
Co2−N3	2.131(4)	Co2−O5	2.143(3)	Co2−N4	2.147(3)	Co2−N2	2.165(4)
Co3−O19	2.042(4)	Co3−O20	2.051(4)	Co3−N7	2.135(4)	Co3−N6	2.162(4)
Co3−N8	2.166(3)	Co3−N5	2.180(3)	Co4−O21	2.072(4)	Co4−O12	2.104(4)
Co4−N10	2.138(4)	Co4−N11	2.163(4)	Co4−N14#1	2.170(4)	Co4−N9	2.210(4)
O16−Co1−N12	78.23(13)	O1−Co1−N1	78.52(12)	N3−Co2−N2	77.95(13)	O5−Co2−N4	77.09(12)
N7−Co3−N8	78.02(14)	N6−Co3−N5	78.24(14)	O12−Co4−N9	76.84(13)	N10−Co4−N11	77.09(14)
				3			
Ni1−O1	2.063(3)	Ni1−O18	2.066(3)	Ni1−N11	2.093(3)	Ni1−N12	2.099(3)
Ni1−O17	2.103(3)	Ni1−N1	2.152(3)	Ni2−O19	2.023(3)	Ni2−O5	2.061(3)
Ni2−N3	2.096(3)	Ni2−N2	2.132(3)	Ni2−N4	2.147(3)	Ni2−O15#1	2.163(3)
Ni3−O9	2.064(3)	Ni3−N6	2.074(3)	Ni3−O21	2.084(3)	Ni3−O20	2.083(3)
Ni3−N5	2.106(3)	Ni3−N7	2.117(3)	Ni4−O23	2.047(3)	Ni4−O22	2.057(3)
Ni4−O13	2.065(3)	Ni4−N8	2.090(3)	Ni4−N9	2.131(3)	Ni4−N10	2.186(3)
O1−Ni1−N1	79.47(11)	N11−Ni1−N12	78.94(12)	O5−Ni2−N4	79.12(11)	N3−Ni2−N2	79.66(12)
N6−Ni3−N5	79.34(12)	O9−Ni3−N7	79.56(11)	N8−Ni4−N9	80.65(12)	O13−Ni4−N10	78.87(10)
				4			
Ni1−O5	2.044(4)	Ni1−O4#1	2.060(3)	Ni1−N3	2.086(4)	Ni1−N1	2.138(4)
Ni1−N4	2.148(4)	Ni1−N2#1	2.229(4)				
O5−Ni1−O4#1	88.91(16)	O5−Ni1−N3	176.88(16)	O5−Ni1−N1	98.06(15)	O4#1−Ni1−N2#1	78.10(13)
N3−Ni1−N1	79.64(15)	O5−Ni1−N4	88.77(17)	N3−Ni1−N4	89.30(16)	N1−Ni1−N4	94.40(15)
				5			
Cd1−O9	2.210(3)	Cd1−N1	2.258(2)	Cd1−N4	2.263(3)	Cd1−N3	2.335(3)
Cd1−N6	2.382(3)	Cd2−O7#1	2.299(2)	Cd2−O7#2	2.299(2)	Cd2−O4#3	2.330(2)
Cd2−O4	2.330(2)	Cd2−N2	2.355(2)	Cd2−N2#3	2.355(2)	Cd3−O1#4	2.307(2)
Cd3−O1#5	2.307(2)	Cd3−O8	2.349(2)	Cd3−O8#3	2.349(2)	Cd3−N5	2.372(2)
N1−Cd1−N3	72.92(9)	N4−Cd1−N6	72.17(9)	O9−Cd1−N3	115.87(10)	O4−Cd2−N2	71.77(8)
O7#1−Cd2−N2	158.06(9)	O8−Cd3−N5	71.16(8)	O1#4−Cd3−N5	126.13(8)	O8−Cd3−O8#3	150.78(11)

[a] Symmetry transformations used to generate equivalent atoms: for **1**, #1, $-x, y, -z+{}^1/_2$; for **2**, #1, $-x, y, -z+{}^1/_2$; for **3**, #1, $-x+1, y-{}^1/_2, -z+{}^3/_2$; for **4**, #1, $-y+{}^5/_4, x+{}^1/_4, -z+{}^1/_4$; for **5**, #1, $x+{}^1/_2, y+{}^1/_2, -z+{}^1/_2$; #2, $-x+{}^1/_2, y+{}^1/_2, z$; #3, $-x+1, y, -z+{}^1/_2$; #4, $x, -y, z+{}^1/_2$; #5, $-x+1, -y, -z$.

Table 3. Hydrogen Bonds of Complex **3**[a]

D−H···A	*d*(D−H) (Å)	*d*(H···A) (Å)	*d*(D···H) (Å)	∠(D−H···A) (deg)
O18−H18A···O24	0.854(10)	1.96(2)	2.783(7)	161(5)
O19−H19A···O4	0.84	1.77	2.608(5)	171.9
O21−H21A···O8	0.84	1.79	2.595(4)	160.4
O23−H23B···O12	0.81(5)	1.77(5)	2.579(4)	172(5)
O17−H17A···O3#3	0.84	2.11	2.887(5)	153.1
O23−H23A···O1#3	0.84	1.91	2.657(4)	147.5
O18−H18B···O21#4	0.856(10)	2.19(2)	2.986(4)	155(5)
O19−H19C···O9#5	0.867(5)	2.17(5)	2.860(4)	137(4)
O20−H20A···O16#6	0.84	1.87	2.702(4)	173.9
O20−H20B···O5#7	0.852(10)	2.00(2)	2.807(4)	158(5)
O21−H21C···O12#8	0.861(10)	2.08(2)	2.874(4)	154(5)
O22−H22A···O8#9	0.84	1.91	2.716(4)	159.2

[a] Symmetry codes: #3, $-x, y+{}^1/_2, -z+{}^3/_2$; #4, $-x+{}^1/_2, -y+1, z-{}^1/_2$; #5, $x+{}^1/_2, -y+{}^1/_2, -z+2$; #6, $-x+{}^1/_2, -y+1, z+{}^1/_2$; #7, $x-{}^1/_2, -y+{}^1/_2, -z+2$; #8, $x+{}^1/_2, -y+{}^3/_2, -z+2$; #9, $x-{}^1/_2, -y+{}^3/_2, -z+2$.

Crystal Structures of 1 and 2. Complexes **1** and **2** are discrete octanuclear aggregates. They are isomorphous structures crystallized in the monoclinic space group *C*2/*c*. Thus, only the structural feature of **1** is discussed

Scheme 1. Schematic Structure and Coordination Modes of Ligand H_3L

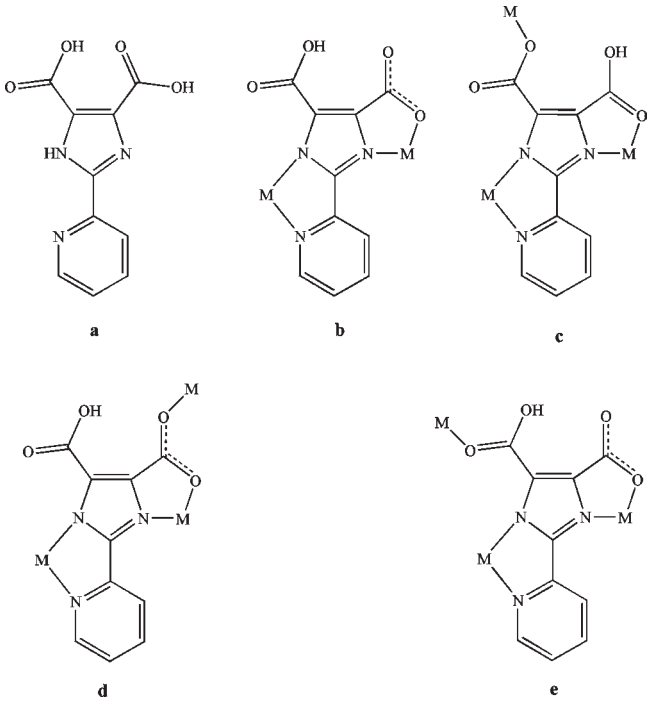

representatively. Complex **1** comprises $Ni_4(HL)_4$ metallacalix[4]arene building blocks further bridged by bpy. Figure 1 illustrates two different cavities: the $Ni_4(HL)_4$ metallacalix[4]arene building blocks and the cavity constructed by bpy-bridged adjacent $Ni_4(HL)_4$ metallacalix[4]arene building blocks. Each $Ni_4(HL)_4$ unit consists of four crystallographically independent Ni^{II} ions cyclized in a bichelating fashion by four HL ligands, with the linkage style between Ni^{II} ions and ligands HL being the A mode (Scheme 2). Each Ni^{II} ion is in a slightly distorted octahedral coordination geometry, but their coordination spheres are very different. Ni1 is ligated by two HL ligands via N,O-heterochelation, one terminal water molecule, and a μ-bpy, while Ni2 is in the coordination geometry of N_4O_2 constructed by one HL via N,O-heterochelation, one HL via N,N-homochelation, one terminal water molecule, and one py. The N_4O_2 coordination geometry for Ni3 is fabricated by two HL ligands via N,N-homochelation and two terminal water molecules, whereas that for Ni4 is built from one HL via N,O-heterochelation, one HL via N,N-homochelation, one terminal water molecule, and a μ-bpy. Ni−N and Ni−O bonds fall in the normal ranges of 2.075(4)−2.179(3) and 2.022(3)−2.089(3) Å, respectively. Each HL in a μ-kN,N′:kO,N″ mode (Scheme 1b) chelates two individual Ni^{II} ions to form two five-membered rings with dihedral

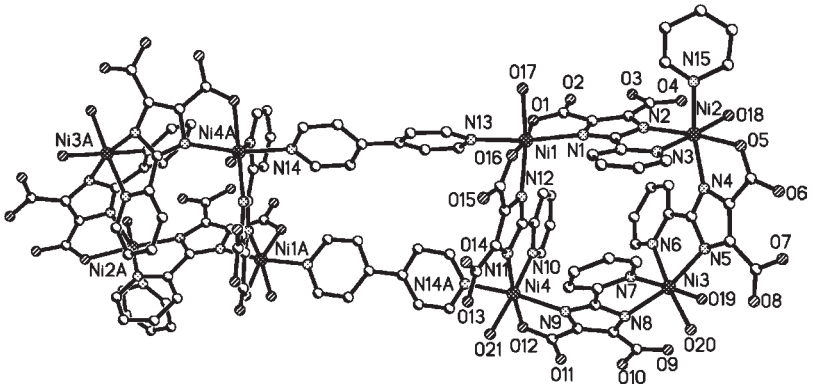

Figure 1. View of a bpy-bridged octanuclear nanostructure in **1**, containing C_1-symmetric $Ni_4(HL)_4$ metallacalix[4]arene building blocks in the A linkage mode and showing two sorted cavities.

Scheme 2. View of the Linkage Styles between the Metal Nodes and HL Ligands in $M_4(HL)_4$ Building Blocks

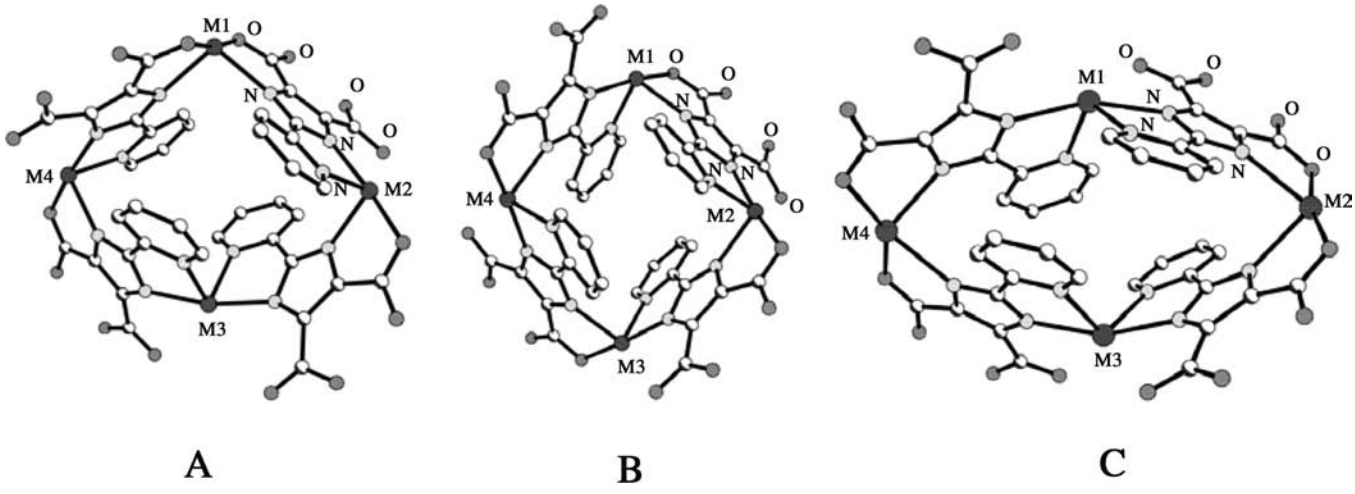

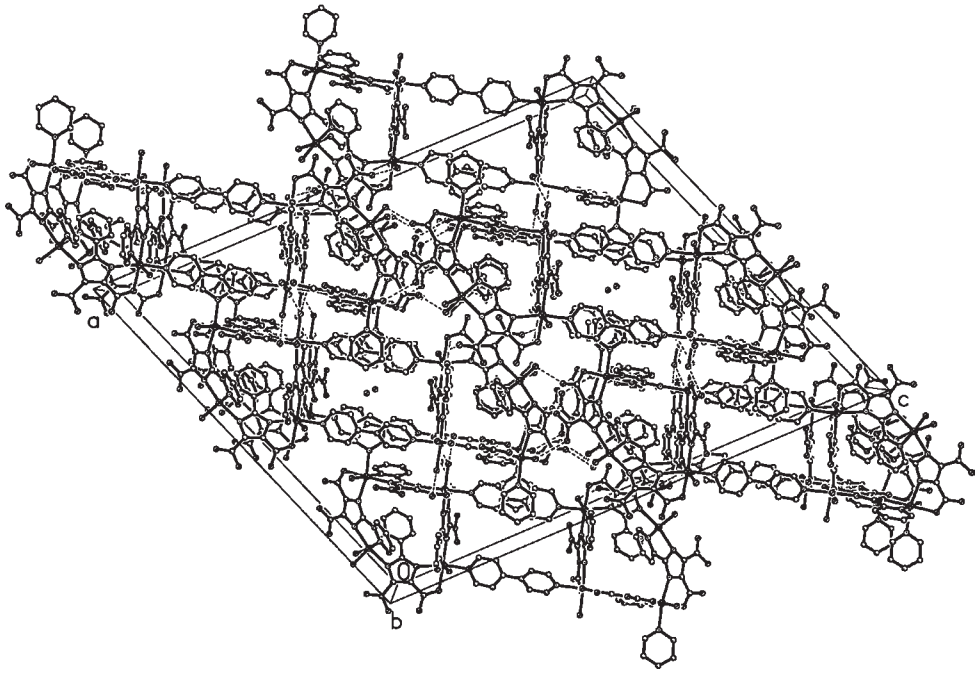

Figure 2. View of the same sorted cavities running through to form 1D channels along the *b* axis through $\pi\cdots\pi$ interactions and hydrogen bonding in **1**, with the lattice water residing in the larger channels.

angles ranging between 3.6 and 28.5°, showing the cooperative coordination orientation between the 4,5-imidazoledicarboxylate and 2-pyridyl groups, which is different from the μ-*k*O,N:*k*O′,N′ chelating mode of H_3IDC.[6] In the $Ni_4(HL)_4$ unit, the four Ni^{II} ions are almost coplanar, with the mean deviation from the least-squares plane being 0.0845 Å, and the four bichelating HL ligands with the adjacent HL being oppositely directed are cleft by the plane, with their carboxylic and 2-pyridyl groups being regularly up and down. Notably, the $Ni_4(HL)_4$ metallacalix[4]arene building block merely possesses C_1 symmetry. The great distortion of the $Ni_4(HL)_4$ unit is indicated by the fact that (i) the dihedral angles relating to the two five-membered chelating rings common to the same vertex cover the range of 81.4−94.7°, (ii) Ni···Ni···Ni angles and Ni···Ni distances along the edges are in the ranges of 78.09−104.34° and 6.049−6.286 Å, respectively, and (iii) four HL ligands with their 2-pyridyl and 4,5-imidazoledicarboxylate groups bending entad and forth, respectively, surround an irregular cage with dimensions of ca. 7.780 × 9.564 × 9.425 $Å^3$. It should mentioned that the measurement for the cages in all compounds is scaled by the distances of metal center to metal center along the diagonal in the metallacalix[4]-arene building blocks and the length of HL. Through the C_2 symmetry, two $Ni_4(HL)_4$ units are linked to form a discrete octanuclear nanostructure by two μ-bpy ligands. The octanuclear molecule is chiral only with a C_2 axis passing through the cavity constructed by bpy-bridged adjacent $Ni_4(HL)_4$ metallacalix[4]arene building blocks along the *b* axis. The resulting cavity is slightly puckered and larger. It is particularly interesting that the same sorted cavities run through to form 1D channels through $\pi\cdots\pi$ interactions and hydrogen bonding, directing the stacking, as is clearly shown in Figure 2, and the lattice water resides in the larger channels. The percent effective free volume in **1** is 22.7% (a total potential solvent volume of 3078.6 $Å^3$ out of every unit cell volume of 13588.0 $Å^3$) calculated with *PLATON*.[11]

Crystal Structure of 3. Complex **3** crystallized in a chiral space group $P2_12_12_1$ also contains $Ni_4(HL)_4$ metallacalix-[4]arene building blocks created by four crystallographically independent Ni^{II} ions linked in a bichelating fashion by four HL ligands. This $Ni_4(HL)_4$ cryptate is sized at ca. 7.804 × 8.834 × 9.425 $Å^3$. In the $Ni_4(HL)_4$ unit, the four Ni^{II} ions obviously deviate from the least-squares plane by 0.9892 Å to form a puckered square, with Ni···Ni··· Ni angles lying between 77.30 and 90.76° and Ni···Ni distances along the edges being in the range of 6.154−6.258 Å, and each Ni^{II} ion chelates to two HL ligands via N,O-heterochelation and N,N-homochelation, respectively, to fabricate two five-membered chelating rings, incompletely similar to those in **1** and **2** (Figure 3). In a sense, they are isomeric metallacalix[4]arene building blocks (Scheme 2B). To finish a N_3O_3 slightly distorted octahedral geometry, each Ni^{II} ion additionally ligated by two oxygen atoms from two water molecules or one water molecule and one unchelating carboxyl group of one HL. Ni−N and Ni−O bonds cover the ranges of 2.074(3)−2.186(3) and 2.023(3)−2.163(3) Å, respectively, similar to those in **1**. In the $Ni_4(HL)_4$ unit, three out of the four HL ligands show the μ-*k*N,N′:*k*O,N″ mode found in **1** (Scheme 1b), while the other presents a μ_3-*k*N,N′:*k*O,N″:*k*O′ mode (Scheme 1c) not only to participate in the formation of the $Ni_4(HL)_4$ unit but also to link the $Ni_4(HL)_4$ units into 2_1 helices with a pitch of 14.426 Å along the *b* axis (Figure 4). Those adjacent helices are interestingly bridged by O17···O3 hydrogen bonding to form a chiral plane. Along the *a* and *c* axes, the $Ni_4(HL)_4$ units also arrange in 2_1 helices through O21···O12 and O20···O16 hydrogen bonding with pitches of 8.347 and

(11) Speck, A. L. *PLATON, A Multipurpose Crystallographic Tool*; Utrecht University: Utrecht, The Netherlands, 2005.

28.924 Å, respectively. Thus, the resulting large chiral building blocks $Ni_4(HL)_4$ assemble into 3D chiral supramolecular crystals with lattice water in the larger channels (Figure 5), although the spontaneous separation results in a racemic compound.

Crystal Structure of 4. Complex **4** crystallizes in a space group $I4_1/a$. The asymmetric unit consists of one Ni^{II}, one HL, half of a bpy, and one coordination water molecule. Through the S_4 symmetry operation, the asymmetric unit produces a comparatively higher symmetric $Ni_4(HL)_4$ metallacalix[4]arene building block with dimensions of ca. $7.870 \times 7.870 \times 9.425$ Å^3, which is very close to the C_{4v} symmetry of a normal calix[4]arene (Figure 6). In the $Ni_4(HL)_4$ unit, four HL ligands, all in the μ-kN,N′:kO,N″ mode, locate the four Ni^{II} ions at the vertices of a S_4-symmetric tetrahedron, with all of Ni···Ni···Ni angle of 77.47° and Ni···Ni distances along the edges being 6.289 Å, and each Ni^{II} ion chelates to two HL ligands to fabricate two five-membered chelating rings with a dihedral angle of 88.8°. To finish a N_4O_2 slightly distorted octahedral geometry, the Ni^{II} ion is additionally ligated by one oxygen atom from water and a nitrogen atom from bpy. Ni−N and Ni−O bonds cover the ranges of 2.086(4)−2.229(4) and 2.044(4)−2.060(3) Å, respectively. Notably, along the c axis the $Ni_4(HL)_4$ metallacalix[4]arene building blocks are arranged to form bpy-bridged 4_1 helices with large pitches of 39.336 Å (Figure 7a). As is intriguingly shown in Figure 7b, those wound 4_1 helices further extend into a diamondoid framework through pillars μ-bpy. To the best of our knowledge, the diamondoid architecture with metallacalix[4]arene building blocks as novel 4-connecting nodes is authentically rare.[12] Unluckily, the spacious voids are filled via the mutual interpenetration of four independent equivalent frameworks. The resulting 3D 5-fold interpenetrating crystal material with channels of a free opening of ca. 6.006×6.247 Å^2 along the a and b axes is presented in Figure 8, and the percent effective free volume is still of 31.6% (a total potential solvent volume of 2456.6 Å^3 out of every unit cell volume of 7783.9 Å^3) calculated with *PLATON*.

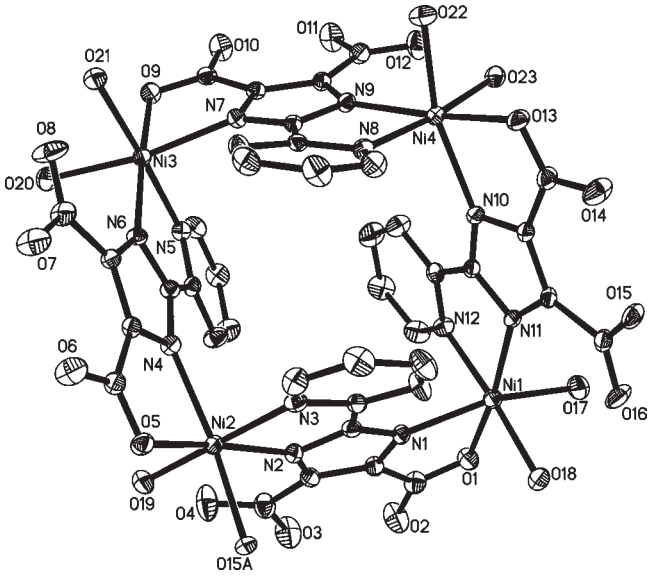

Figure 3. ORTEP representation of a pseudo-S_4-symmetric $Ni_4(HL)_4$ metallacalix[4]arene building block in the B linkage mode in **3**.

Crystal Structure of 5. The asymmetric unit of **5** comprises one Cd^{II}, two halves of Cd^{II}, two HL ligands, and one coordinated water molecule. A C_2 axis passes through the two halves of Cd^{II} centers, thereby creating a compressed $Cd_4(HL)_4$ metallacalix[4]arene building block with dimensions of ca. $6.343 \times 11.502 \times 9.425$ Å^3, clearly presented in Figure 9. Surely, the $Cd_4(HL)_4$ metallacalix[4]arene building block only has C_2 symmetry, and four Cd^{II} ions are regularly located at the vertices of a rhombus, with Cd···Cd···Cd angles being 58.00 and 122.24° and Cd···Cd distances along the edges being 6.542 and 6.593 Å. Through the same bichelating fashion of HL as that found in compounds **1**−**4**, four Cd^{II} centers are bridged to form the $Cd_4(HL)_4$ unit of **5**, but their linkage styles between the metal nodes and HL ligands are very different (Scheme 2C). In **5**, five-coordinated Cd1 in a sharply distorted trigonal bipyramid is ligated by two HL ligands via N,N-homochelation and one water molecule, and a dihedral angle between the resulting five-membered chelating rings is 64.1°. While six-coordinated Cd2 in a sharply distorted octahedron, with a

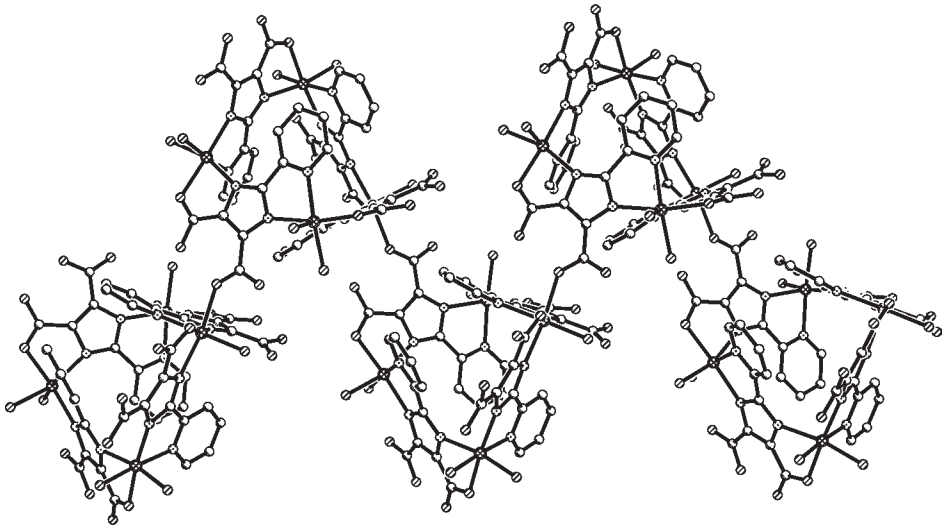

Figure 4. View of 2_1 helices with a pitch of 14.426 Å constructed from $Ni_4(HL)_4$ building blocks in **3**.

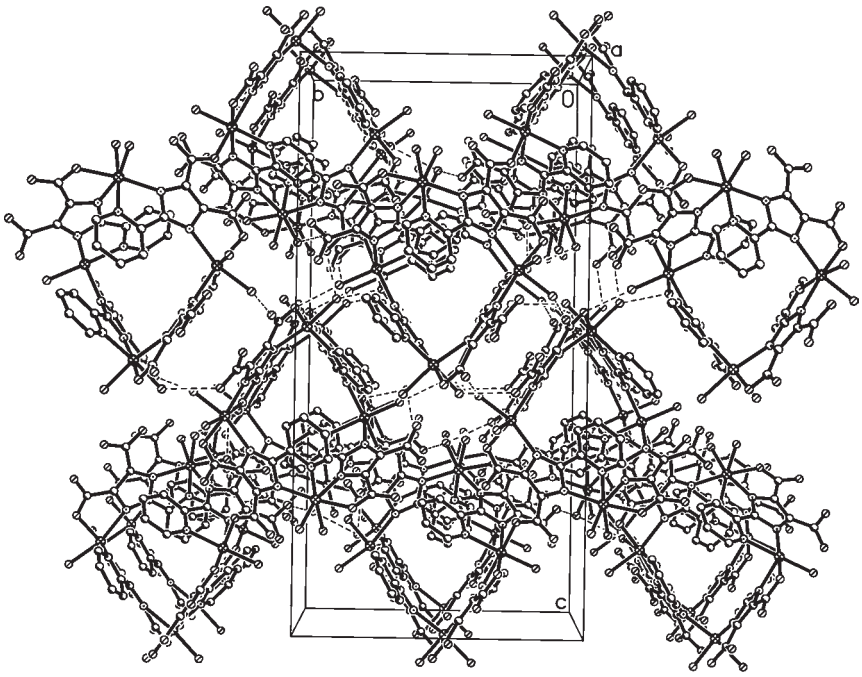

Figure 5. View of a hydrogen-bonded 3D chiral network containing 2_1 helices with various interesting apertures in **3**.

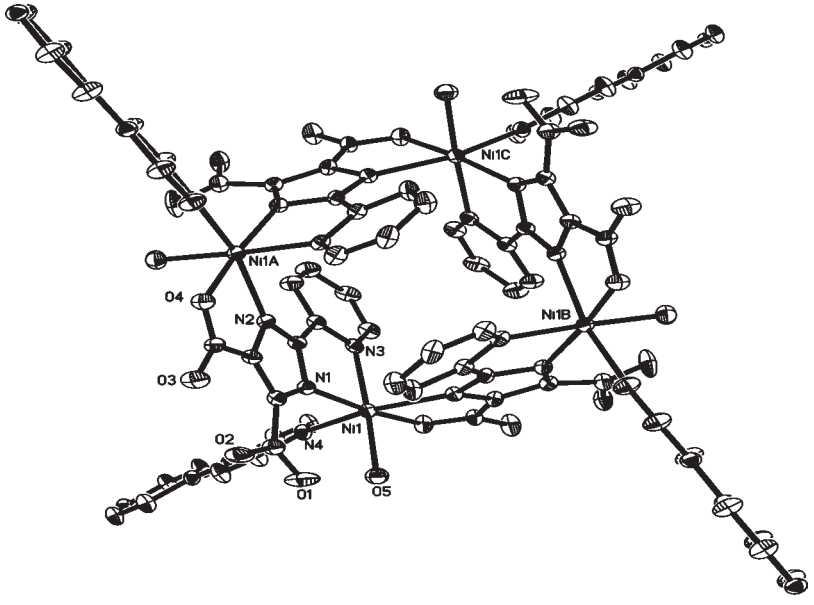

Figure 6. ORTEP representation of a S_4-symmetric $Ni_4(HL)_4$ building block in the B linkage mode in **4**, showing a bpy-bridged 4-connector.

dihedral angle of the chelating ring being 68.9°, or six-coordinated Cd3 in a slightly distorted trigonal prism, with a dihedral angle of the chelating ring being 51.5°, is coordinated by two HL ligands via N,O-heterochelation and two HL ligands via monocoordination of the carboxyl. Cd−N and Cd−O bonds cover the normal ranges of 2.258(2)−2.382(3) and 2.210(3)−2.349(2) Å, respectively. Outstandingly, the two HL ligands in the asymmetric unit of **5** both act as 3-connectors to form the $M_4(HL)_4$ unit in a bichelating fashion and to bridge the adjacent $Cd_4(HL)_4$ unit through further coordination of the carboxyl groups but possess different coordination modes: one uses the coordination of another oxygen atom in the carboxyl via N,O-heterochelation to link the adjacent $Cd_4(HL)_4$ unit, while the other uses that in the unchelated carboxyl group (Scheme 1d,e). In this way, the $Cd_4(HL)_4$ units extend into a 3D framework with smaller apertures, and the effective free volume is only of 1.7% (a total potential solvent volume of 72.6 $Å^3$ out of every unit cell volume of 4273.2 $Å^3$) calculated with *PLATON* (Figure 10a). If we simplify the $M_4(HL)_4$ unit as a single node located in the center of the Cd^{II} cluster, the $M_4(HL)_4$ unit becomes an 8-connector. Notably, the 8-connector orients six different

(12) (a) Cheng, J.-K.; Chen, Y.-B.; Wu, L.; Zhang, J.; Wen, Y.-H.; Li, Z.-J.; Yao, Y.-G. *Inorg. Chem.* **2005**, *44*, 3386. (b) Wang, X.-S.; Zhao, H.; Qu, Z.-R.; Ye, Q.; Zhang, J.; Xiong, R.-G.; You, X.-Z.; Fun, H. K. *Inorg. Chem.* **2003**, *42*, 5786.

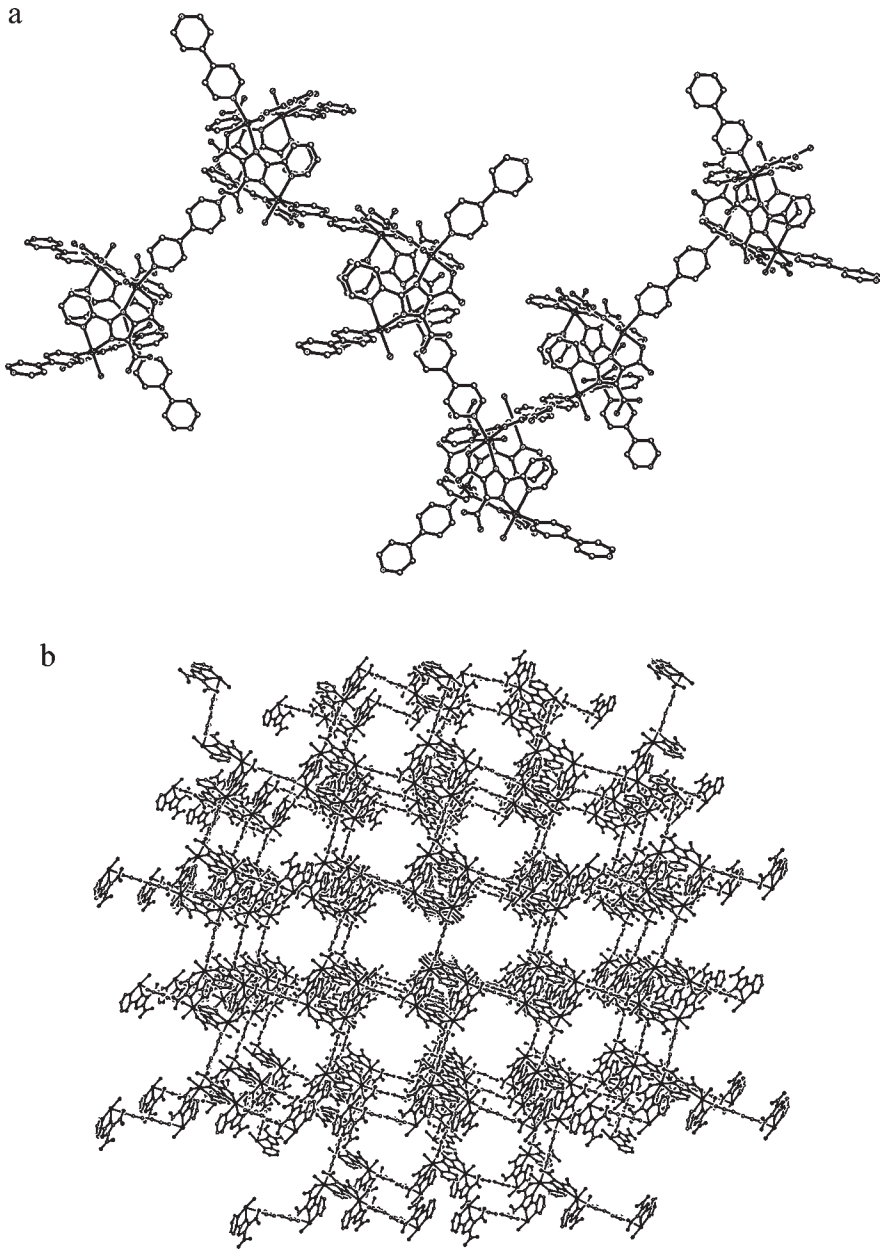

Figure 7. (a) View of bpy-bridged 4_1 helices with a large pitch of 39.336 Å along the *c* axis built from $Ni_4(HL)_4$ building blocks. (b) Diamondoid architecture with metallacalix[4]arene building blocks as novel 4-connecting nodes in **4**.

directions, with some two directions being doubly bonded, and only link to six adjacent $M_4(HL)_4$ units to give the α-Po net with the $4^{12}6^3$ topology symbol (Figure 10b). This example can compare well with other α-Po nets constructed from highly connected secondary building units, such as 12- and 16-connectors, and also represents a novel case that the network is only constructed by a single bridged ligand.[13]

Magnetic Properties. The temperature-dependent magnetic susceptibilities (χ_M) of polycrystalline samples **1**−**4** were measured in the temperature range of 2−300 K, and the corresponding graphs of χ_M and $\chi_M T$ vs T (χ_M for tetranuclear units) are shown in Figure 11a−d, respectively.

For the three nickel(II) complexes **1**, **3**, and **4**, the $\chi_M T$ values showed similar temperature profiles, and the values at 300 K of 4.48−5.18 $cm^3\ mol^{-1}\ K$ are larger than the value (4.00 $cm^3\ mol^{-1}\ K$ with $g = 2$) expected for an uncorrelated sum of four Ni^{II} ions, revealing a certain orbital contribution. The $\chi_M T$ values gradually decreased as the temperature was lowered, followed by a sudden decrease below about 50 K. Meanwhile, the χ_M values for each nickel(II) complex also showed similar temperature profiles, and they reached a maximum value around 16 K. These behaviors suggest the presence of antiferromagnetic interactions. The magnetism similarity is mainly controlled by the existence of almost the same $Ni_4(HL)_4$ metallacalix[4]arene building blocks, where interactions of the tetranuclear Ni^{II} ions are exchanged by ligands HL but subtle differences in the magnetic behaviors are due to the different symmetries of $Ni_4(HL)_4$ and the linkage

(13) (a) Wen, Y.-H.; Zhang, J.; Wang, X.-Q.; Feng, Y.-L.; Cheng, J.-K.; Li, Z.-J.; Yao, Y.-G. *New J. Chem.* **2005**, *29*, 995. (b) Luo, F.; Che, Y.-X.; Zheng, J.-M. *Cryst. Growth Des.* **2006**, *6*, 2432. (c) Yang, Y.-T.; Luo, F.; Che, Y.-X.; Zheng, J.-M. *Cryst. Growth Des.* **2008**, *8*, 3508.

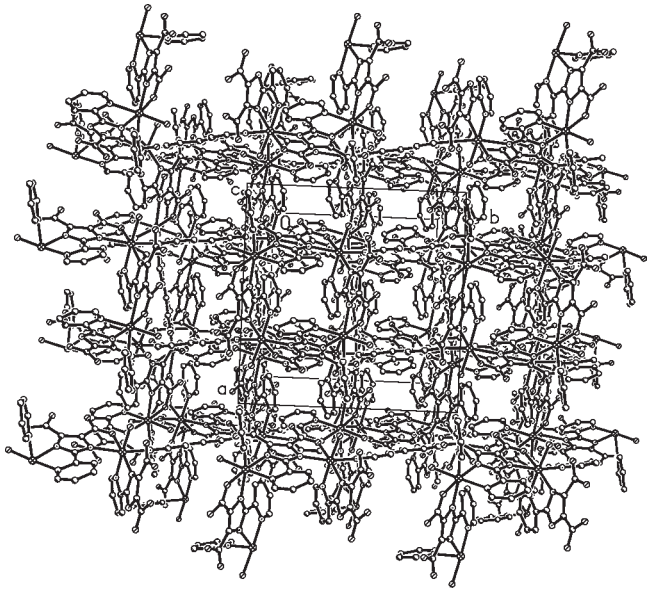

Figure 8. View of the 3D 5-fold interpenetrating diamondoid network in **4**, showing 1D channels reduced by interpenetration along the *c* axis.

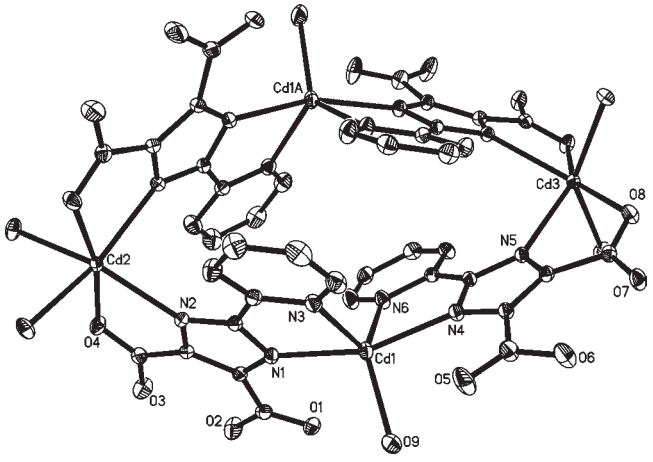

Figure 9. ORTEP representation of a C_2-symmetric, compressed $Cd_4(HL)_4$ building block in the C mode in **5**, showing three Cd^{II} ions with different coordination geometries.

styles between the metal nodes in or between $Ni_4(HL)_4$ and the solid stack, which inversely result in the different amplitudes of *g* values, intratetranuclear exchange coupling constants (*J*), and intertetranuclear magnetic interactions. In the $Ni_4(HL)_4$ building block of **4**, the arrangement of tetranuclear Ni^{II} ions has S_4 symmetry and Ni^{II} ions located at the diagonal vertices are unlinked and well separated. Thus, we further evaluate the magnetic behavior of the novel $Ni_4(HL)_4$ metallacalix[4]arene building block by using the geometry of an equilateral quadrangle, where the spin Hamiltonian takes the form of $\hat{H} = -2J(\hat{S}_1\hat{S}_{1A} + \hat{S}_{1A}\hat{S}_{1B} + \hat{S}_{1B}\hat{S}_{1C} + \hat{S}_{1C}\hat{S}_1)$. Additionally, the tetranuclear clusters are separated by long spacer μ-bpy in the 3D framework, and the comparatively weak intertetranuclear interactions (zJ') are treated under the molecular-field approximation. Consequently, the simplified exchange pathway in and among the tetranuclear clusters is schematically represented in Figure 12 based on which exchange equation (eq S1 in the Supporting Information) was evolved. The best fit of the experimental data of **4** to eq S1 yielded $J = -2.72(3)$ cm^{-1}, $zJ' = -0.98(11)$ cm^{-1}, and $g = 2.20(2)$ with an agreement factor $R = \sum(\chi_{obsd} - \chi_{calcd})^2/\sum\chi_{obsd}^2) = 1.07 \times 10^{-3}$. As for **1**−**3**, the array of tetranuclear Ni^{II} or Co^{II} ions in the C_1-symmetric $M_4(HL)_4$ building block is in a distorted quadrangle, and the cluster topology and connectivity in or among clusters are similar to those of **4**, so the magnetic model for **4** is used to analyze the magnetism of **1**−**3**. For the two nickel(II) compounds **1** and **3**, the experimental data of magnetic susceptibility can be well fitted by eq S1 with $J = -4.00(2)$ cm^{-1}, $zJ' = -0.98(11)$ cm^{-1}, $g = 2.29(1)$, and $R = 5.63 \times 10^{-4}$ for **1** and $J = -3.39(2)$ cm^{-1}, $zJ' = -1.16(11)$ cm^{-1}, $g = 2.36(2)$, and $R = 7.00 \times 10^{-4}$ for **3**. Notably, the cobalt(II) complex **2** is the isomorphous structure of **1**, but its magnetic susceptibility is unsuccessfully reproduced by eq S2 (Supporting Information) built from the equilateral quadrangle isotropic model combined with the molecular-field approximation due to the complexity of the magnetic anisotropy originating from the spin−orbit coupling and axial distortion.[14] As shown in Figure 11b, the $\chi_M T$ value of polycrystal sample **2** at 300 K is 11.55 cm^3 mol^{-1} K, which is obviously larger than the value (7.50 cm^3 mol^{-1} K with $g = 2$) expected for an uncorrelated sum of four Co^{II} ions, revealing a typical contribution of the orbital momentum for the $^4T^1{}_g$ ground state. Upon cooling, $\chi_M T$ gradually decreases to a value of 9.00 cm^3 mol^{-1} K at 65 K and then dramatically decreases to 1.11 cm^3 mol^{-1} K at 2 K. The $\chi_M{}^{-1}$ vs *T* plot is essentially linear, and least-squares fitting of the data to the Curie−Weiss law gives $C = 12.10(3)$ cm^3 mol^{-1} K and $\theta = -19.98(11)$ K (Figure S1 in the Supporting Information). The negative value of θ shows quite weak antiferromagnetic interactions in the $Co_4(HL)_4$ building block, which is in agreement with the curve of $\chi_M T$ vs *T* and no maximum observed in χ_M.[15]

Photoluminescence Properties. The solid-state photoluminescent spectra of **5** and free ligand H_3L at room temperature are depicted in Figure 13. Free ligand H_3L is strongly photoluminescent and exhibits an intense blue emission with a single broad band at $\lambda_{max} = 452$ nm, corresponding to excitation at $\lambda_{max} = 370$ nm. Not only the emission wavelength but also the intensity of H_3L is very similar to that of analogue H_3PIDC, which exhibits a blue photoluminescence with $\lambda_{max} = 462$ nm upon excitation at 380 nm (Figure S2 in the Supporting Information). When excited at 352 nm, complex **5** displays an emission at $\lambda_{max} = 396$ nm with an obvious blue shift of 56 nm and a sharp emission intensity attenuation of about two-third compared to that of H_3L. Probably, the emission nature of **5** is mainly due to a ligand-centered emission state including the significant charge-transfer character induced by the polar cation, as reported for Cd^{II} or other d^{10} metal complexes with N-donor ligands based

(14) (a) Kahn, O. *Molecular Magnetism*; VCH: New York, 1993. (b) Jensen, P.; Batten, S. R.; Moubaraki, B.; Murray, K. S.; Robson, R. *J. Solid State Chem.* **2001**, *159*, 352. (c) Sakiyama, H.; Ito, R.; Kumagai, H.; Inoue, K.; Sakamoto, M.; Nishida, Y.; Yamasaki, M. *Eur. J. Inorg. Chem.* **2001**, 2027. (d) Sun, H.-L.; Wang, Z.-M.; Gao, S. *Inorg. Chem.* **2005**, *44*, 2169.

(15) (a) Telfer, S. G.; Sato, T.; Kuroda, R.; Lefebvre, J.; Leznoff, D. B. *Inorg. Chem.* **2004**, *43*, 421. (b) Sun, J. S.; Zhao, H.; Ouyang, X.; Clerac, R.; Smith, J. A.; Clemente-Juan, J. M.; Gomez-Garcia, C.; Coronado, E.; Dunbar, K. R. *Inorg. Chem.* **1999**, *38*, 5841.

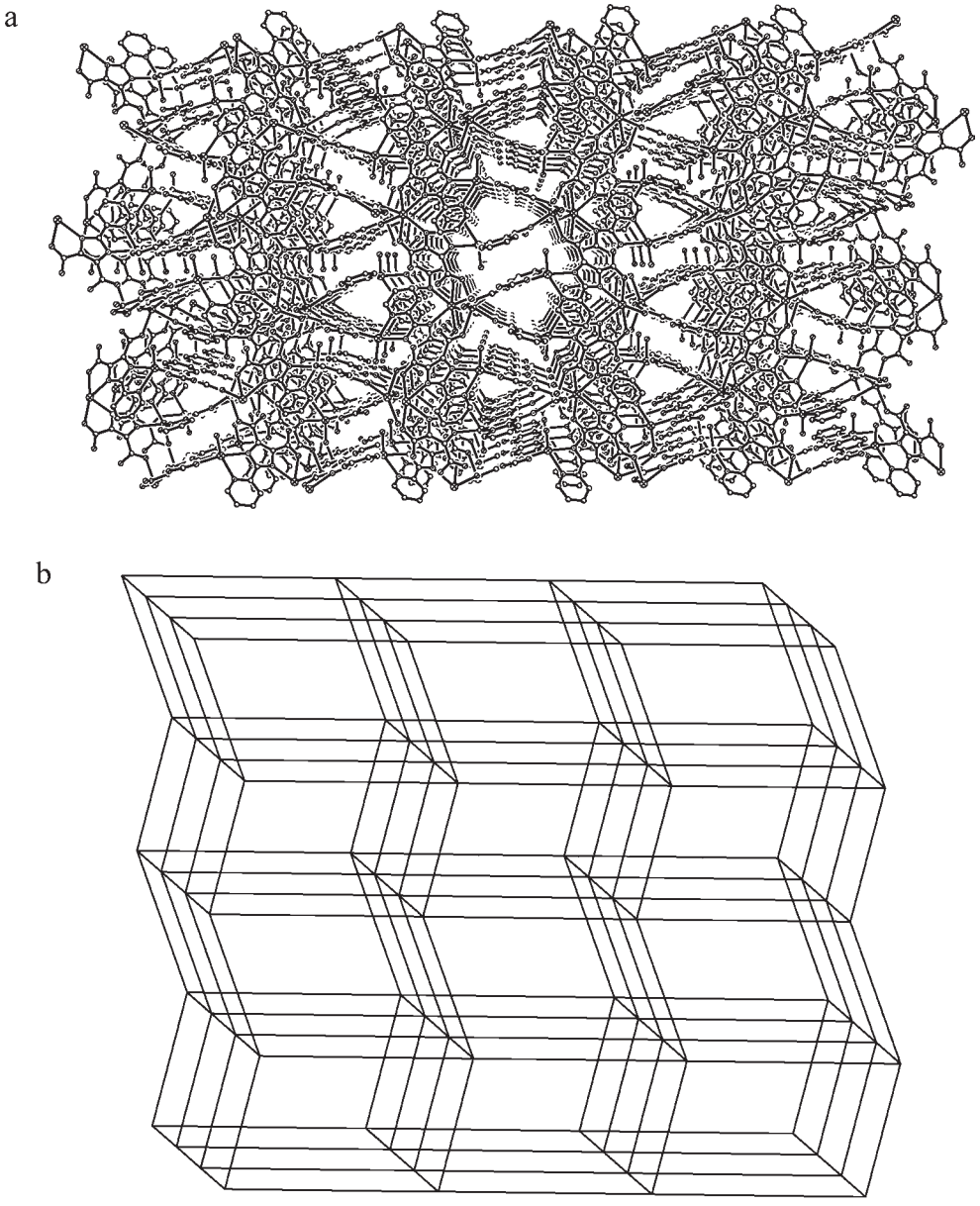

Figure 10. (a) View of a 3D α-Po framework with smaller apertures self-assembled by $Cd_4(HL)_4$ building blocks as 8-connectors. (b) Schematic representation of the α-Po net in **5**.

on the position and shape of the emission band.[16] Remarkably, the emission of **5** is very different from the emission of another cadmium(II) complex $[Cd(HPIDC)(H_2O)]_n$ with the above-mentioned analogue H_3PIDC. The metal-perturbed intraligand emission of $[Cd(HPIDC)(H_2O)]_n$ with λ_{max} = 451 nm upon excitation at 394 nm only undergoes a very slight blue shift compared with that of ligand H_3PIDC with λ_{max} = 462 nm. However, its intensity increases twice much because of chelation of the ligand to the metal center in the 3D framework, which increases the rigidity of $HPIDC^{2-}$ and reduces the nonradiative relaxation process (Figure S2 in the Supporting Information). The analogous ligands are almost similar in their structure and emission nature, but what results in the notable emission difference of their 3D cadmium(II) coordination polymers in both the emission wavelength and intensity? Generally, the metal-perturbed intraligand fluorescent emission wavelength of transition-metal complexes with multipyridyl ligands is mainly related to the extent of π conjugation of the ligands and the emission intensity, which is moderately reduced by coordination water increases with the ligands' conformational rigidity.[17] Structurally, both complexes have coordination water, with ratios of water molecules via Cd^{II} ions in **5**

(16) (a) Han, L.; Hong, M. C.; Wang, R.-H.; Luo, J.-H.; Lin, Z.-Z.; Yuan, D.-Q. *Chem. Commun.* **2003**, 2580. (b) Zhang, J.; Gao, S.; Che, C.-M. *Eur. J. Inorg. Chem.* **2004**, 956. (c) Zheng, C.-G.; Xie, Y.-L.; Xiong, R.-G.; You, X.-Z. *Inorg. Chem. Commun.* **2001**, *4*, 405. (d) Zhang, J.; Xie, Y.-R.; Ye, Q.; Xiong, R.-G.; Xue, Z.-L.; You, X.-Z. *Eur. J. Inorg. Chem.* **2003**, 2572. (e) Luo, J.-H.; Hong, M.-C.; Wang, R.-H.; Cao, R.; Han, L.; Lin, Z.-Z. *Eur. J. Inorg. Chem.* **2003**, 2705.

(17) (a) Perkovic, M. W. *Inorg. Chem.* **2000**, *39*, 4962. (b) Wu, B.-L.; Yuan, D.-Q.; Jiang, F.-L.; Wang, R.-H.; Han, L.; Zhou, Y.-F.; Hong, M.-C. *Eur. J. Inorg. Chem.* **2004**, 2695. (c) Sazanovich, I. V.; Kirmaier, C.; Hindin, E.; Yu, L.; Bocian, D. F.; Lindsey, J. S.; Holten, D. *J. Am. Chem. Soc.* **2004**, *126*, 2665. (d) Aoki, S.; Kagata, D.; Shiro, M.; Takeda, K.; Kimura, E. *J. Am. Chem. Soc.* **2004**, *126*, 13377.

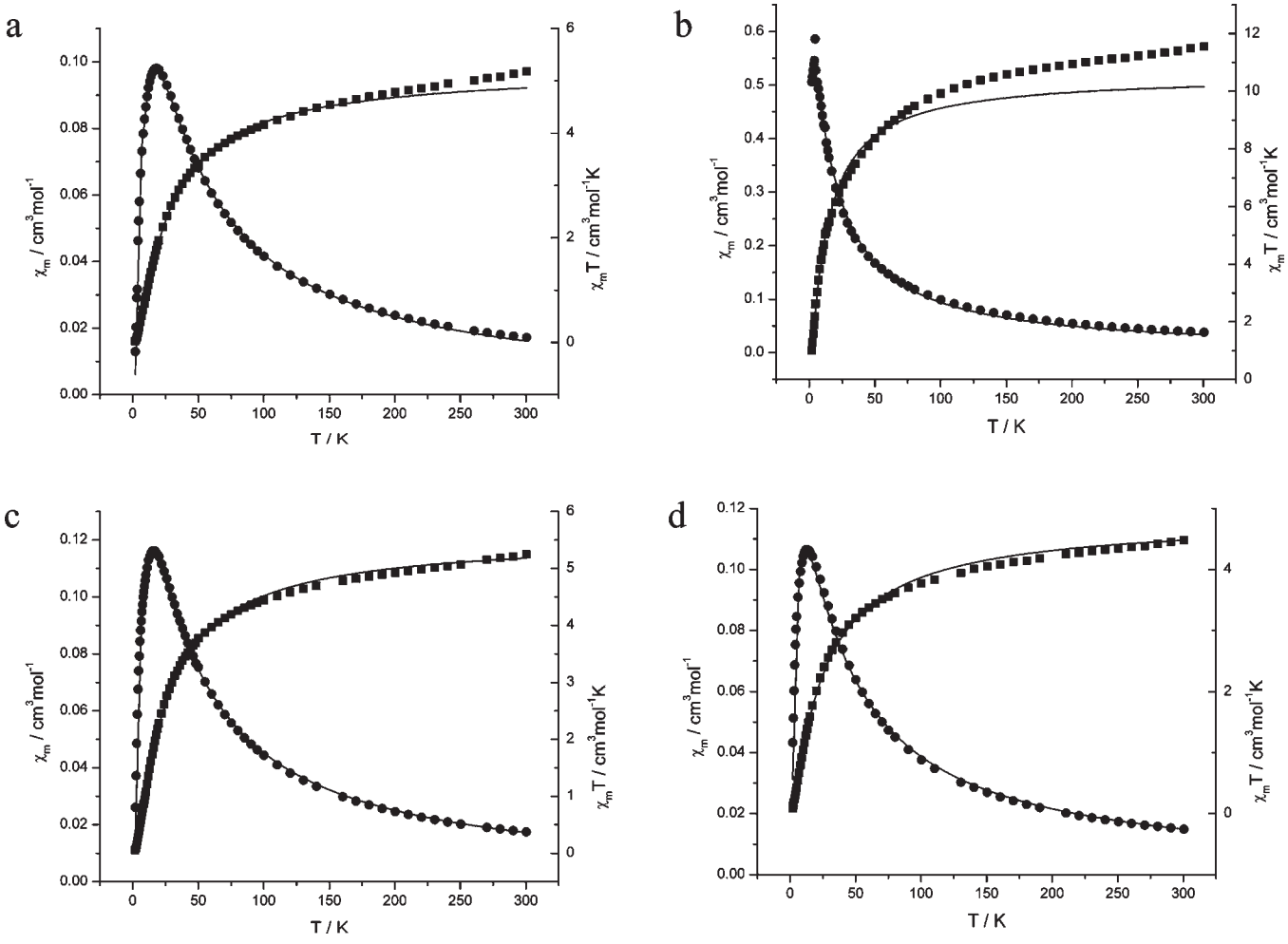

Figure 11. χ_M (●) vs T plot with the theoretical fit (—) and (■) $\chi_M T$ vs T plot with the theoretical fit (—) for **1** (a), **2**(b), **3**(c), and **4** (d).

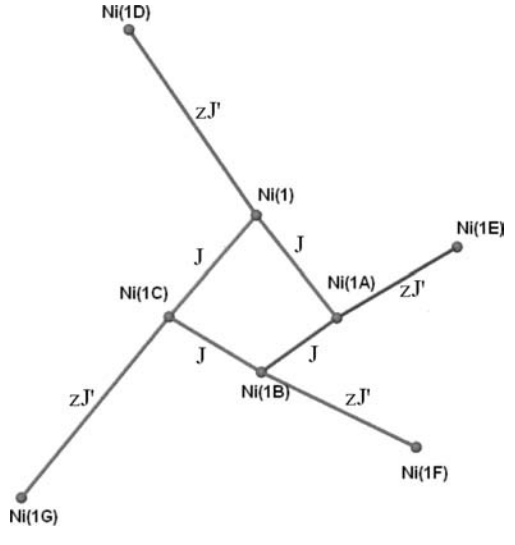

Figure 12. Simplified exchange pathway in and among the tetranuclear clusters in **4**.

and $[Cd(HPIDC)(H_2O)]_n$ being 0.5 and 1, respectively, and every HL^{2-} anion in **5** is firmly bound to Cd^{II} in the α-Po nets through the coordination mode of μ_3-*k*N,N′:*k*O,N″:*k*O′, with its resulting dihedral angles of imidazole ring and pyridine groups being 9.2−10.8°, while each $HPIDC^{2-}$ anion adopts a μ_4-*k*N,O:*k*O:*k*O′:*k*N′ mode to bridge four Cd^{II} atoms in the 3D MOF, with its resulting dihedral angle of the imidazole ring and pyridine being 39.2°. Consequently, the metal-perturbed intraligand emission wavelength of **5** should be close to that of H_3L because that of $[Cd(HPIDC)(H_2O)]_n$ is close to that of H_3PIDC, and its emission intensity would be markedly enhanced. The obvious deviation of the experimental emission of **5** from the above judgment prompts a further comparison between their fine structures, especially including the coordination modes of Cd^{II} and ligands. In $[Cd(HPIDC)(H_2O)]_n$, each Cd^{II} is in a slightly distorted octahedral geometry and every ligand HPIDC has its two carboxyl groups to be deprotonated and monochelates with Cd^{II} through N,O of the 4,5-imidazoledicarboxylic group. However, there are three coordinated type Cd^{II} ions in **5**: five-coordinated Cd1 in a sharply distorted trigonal bipyramid or square pyramid with the coordination water at the vertex, six-coordinated Cd2 in a sharply distorted octahedron, and six-coordinated Cd3 in a slightly distorted trigonal prism. Each ligand HL has the imidazole group and one carboxyl group to be deprotonated and bichelates with Cd^{II} through N,O of the 4,5-imidazoledicarboxylic group and N,N of the imidazole and 2-pyridyl groups (shown in Scheme 1d,e). Perhaps the bichelating fashion of HL, which results in deprotonation of the imidazole group but not the other carboxyl group, exerts a key influence upon the emission

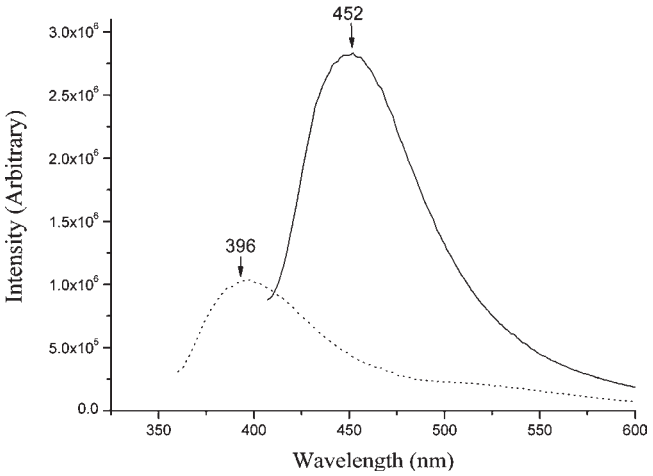

Figure 13. Solid-state photoluminescent spectra of **5** (dotted line) and free ligand H_3L (solid line) at room temperature.

nature of **5**. On the one hand, the bichelating mode, which leads to the almost coplane of the imidazole and 2-pyridyl groups, will make the emission wavelength approach that of ligand H_3L and increase the emission intensity. On the other hand, this mode boosts the electronic delocalization in the ligand's backbone and charge transfer to the metal center and thus greatly effects the molecule orbits and the energy gap between π^* and π molecule orbits of HL and finally results in an obvious blue shift. As for the great decrease of the emission intensity of **5**, it maybe originates from the rare five-coordinated trigonal bipyramid or square pyramid for Cd^{II}, where the vertical coordination water more easily consumes energy through thermal vibration than it does in a normal octahedron.

Thermal Stability and Gas Adsorption. To examine the thermal stability of these networks, thermal gravimetric analyses (TGA; Figure S3 in the Supporting Information) were carried out under an air atmosphere with a flow rate of 60 mL min^{-1} and a heating rate of 10 °C min^{-1}. The decomposition behaviors of isomorphous structures **1** and **2** are very similar. The TGA curves of **1** and **2** indicate the slow release of water molecules (guest water and coordinated water) from 30 to 185 °C to give their dehydrated forms with a first weight loss of 6.2% (calcd 6.3%). At 185 °C, the larger ligand molecules such as py start to be released, and sharp weight losses for **1** and **2** occur at 377 and 393 °C, respectively. For **3**, the slow release of water molecules (guest water and coordinated water) from 33 to 245 °C gives its dehydrated form with a first weight loss of 11.1% (calcd 11.0%). Upon further heating, the main building block of the compound starts to decompose. The framework of **5** decomposes at 280 °C, with a sharp weight loss being observed between 280 and 541 °C. The results of TGA show that the main frameworks of these compounds are rather stable, although accompanied with a slow dehydrated process in a long temperature range.

Compounds **1** and **3** were selected to explore the porosity of these complexes containing metallacalix[4]arene building blocks. On the basis of TGA (vide supra), the crystal samples of **1** and **3** were dried under a high vacuum at 120 °C for 10 h to remove the guest molecules, and

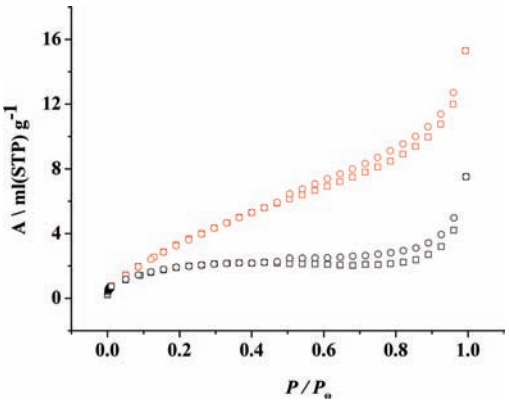

Figure 14. Isotherms of dehydrated **1** (red) and **3** (gray) for the adsorption (squares) and desorption (circles) of nitrogen at 77 K (A = absolute adsorption; STP = standard temperature and pressure).

further PXRD measurements (Figure S4 in the Supporting Information) indicate that the solids after removal of the solvent molecules by heating at 120 °C under vacuum for 10 h retain the initial frameworks of **1** and **3**. The calculated PXRD patterns from the single-crystal X-ray data are in good agreement with the observed ones, and the slight shift and splitting of the peaks may be attributed to the removal of solvent molecules. A determinate quanity of the dehydrated samples **1** and **3** was placed in the quartz tubes and the nitrogen adsorption behaviors at 77 K were measured; a nitrogen adsorption isotherm was taken using automatic volumetric adsorption equipment (ASAP2010, Shimadzu). Complex **1** possesses a Brunauer−Emmett−Teller (BET) surface area of 16.4 m^2 g^{-1}, and the micropore volume is 0.024 cm^3 g^{-1}. For **3**, the measured BET surface area and micropore volume are 7.04 m^2 g^{-1} and 0.012 cm^3 g^{-1}, respectively. The surface areas observed for **1** and **3** are obviously smaller compared with their percent effective free volume calculated with *PLATON* (vide infra). As shown in Figure 14, approximately 15.3 and 7.5 mL of nitrogen were respectively adsorbed per 1.0 g of dehydrated samples **1** and **3** at 1 atm, exhibiting certain adsorptions of nitrogen. The adsorption isotherm clearly indicates no occlusion except the surface adsorption, and thereby the N_2 molecules perhaps are not diffusing into the micropores. Following the same activation process at 120 °C, further adsorption measurements of the dehydrated complex **1** had been done to try adsorption for smaller molecules of H_2 at 77 K and of CO_2 at a higher temperature of 195 K. As shown in Figure S5 in the Supporting Information, about 7.5 mL of H_2 and 7.8 mL of CO_2 were adsorbed per 1.0 g of the dehydrated sample **1** at 800 mmHg and 1 atm, respectively, indicating the poor ability to incorporate guest molecules even for smaller guest molecules or at a higher temperature.

Conclusion

Five intriguing nanostructures and networks consisting of novel metallacalix[4]arene building blocks $M_4(HL)_4$ have been successfully synthesized under hydrothermal conditions. The symmetry of $M_4(HL)_4$ and the linkage styles between the metal nodes and HL ligands in $M_4(HL)_4$ are sensitive to the reaction conditions. In **1** and **2**, two C_1-symmetric $M_4(HL)_4$

units are bpy-bridged to form dimeric octanuclear chiral nanomolecules with two different cavities. As deprotonated with NaOH, the combination of Ni^{II} and HL forms a pseudo-S_4- or S_4-symmetric $M_4(HL)_4$, which further assembles into the 1D chiral crystals **3** with various apertures or the bpy-bridged 3D 5-fold interpenetrating crystal **4**, and the combination of Cd^{II} and HL forms a 8-conneted C_2-symmetric $M_4(HL)_4$, which fabricates the α-Po net of **5**. Magnetic studies disclose antiferromagnetic interactions in $M_4(HL)_4$ of **1**−**4**. For **1**, **3**, and **4**, all containing isomeric $Ni_4(HL)_4$ units, their magnetic properties can be analyzed in the equilateral quadrangle isotropic model combined with the molecular-field approximation, presenting a stronger comparison between the structure and magnetism. The emission nature of **5** is tentatively attributed to a ligand-centered emission, including significant charge-transfer character, and the obvious deviation in the emission wavelength and intensity can be structurally explained from the bichelating fashion of ligands HL and the rare five-coordinated trigonal bipyramid or square pyramid for Cd^{II} with the vertical coordination water. The main frameworks of these compounds have better thermal stability. Gas sorption measurements show that certain gas adsorption for N_2, H_2, and CO_2 occurs, but the guest molecules are not able to diffuse through the porous structures in dehydrated **1** and **3**, which retain the initial frameworks of **1** and **3**. Meaningfully, the designed ligand H_3L displays the strongly cooperative orientation between the 4,5-imidazoledicarboxylate and 2-pyridyl groups in the fabrication of metallacalix[4]arene building blocks with specially shaped and sized apertures. Those large $M_4(HL)_4$ units are potentially highly connected building blocks in the hierarchical assembly of functional MOFs, which also paves the way for attempts at the synthesis of functional materials based other metallacalixarene building blocks, such as metallacalix[3]arene, metallacalix[6]arene, or metallacalix[8]arene.

Acknowledgment. We gratefully acknowledge financial support from the National Natural Science Foundation of China (Grant 20771094), the Science and Technology Key Task of Henan Province (Grant 0524270061), and the China Postdoctoral Science Foundation (Grant 20070410877). The authors thank Dr. Xiuteng Wang and Professor Song Gao of Peking University for helpful support in magnetic measurements.

Supporting Information Available: X-ray crystallographic data in CIF format, plots of $1/\chi_m$ vs $\chi_m T$ vs T and of intensity vs wavelength, TGA curves, PXRD patterns, H_2 and CO_2 adsorption isotherms, and eqs S1 and S2. This material is available free of charge via the Internet at http://pubs.acs.org.